

## COMMUNICATION

# Counting molecules in nano test tubes: *a method for determining the activation parameters of thermally driven reactions through direct imaging*

Received 00th January 20xx,  
Accepted 00th January 20xx

Kayleigh L. Y. Fung,<sup>a</sup> Stephen T. Skowron,<sup>a</sup> Christopher S. Allen,<sup>b,c</sup> and Andrei N. Khlobystov<sup>a\*</sup>

DOI: 10.1039/x0xx00000x

**A methodology for measurement of activation parameters of a thermally driven chemical reaction by direct imaging and counting reactant molecules has been developed. The method combines the use of single walled carbon nanotubes (SWNTs) as a nano test tube, transmission electron microscopy (TEM) as an imaging tool, and a heating protocol that decouples the effect of the electron beam from the thermal activation. Polycyclic aromatic perchlorocoronene molecules are stable within SWNTs at room temperature, allowing imaging of individual molecules before and after each heating cycle between 500–600 °C. Polymerisation reaction rates can be determined at different temperatures simply by counting the number of molecules, resulting in an enthalpy of activation of 104 kJ mol<sup>-1</sup> and very large entropic contributions to the Gibbs free energy of activation. This experimental methodology provides a link between reactions at the single-molecule level and macroscopic chemical kinetics parameters, through filming the chemical reaction in direct space.**

Reaction kinetics, mechanisms and activation parameters are traditionally studied using spectroscopy or diffraction techniques which provide signals indicating bond breaking and forming, averaged over a large number of molecules (e.g. 10<sup>18</sup>–10<sup>20</sup> molecules reacting at the same time). These measurements of bulk kinetics, while invaluable, provide a view averaged over the number of molecules in the reaction. In contrast, single molecule imaging enables direct visualisation of the individual reaction pathway in direct space.<sup>1</sup> Studying reaction kinetics at the single-molecule level can be achieved using ‘nano test tubes’, a concept that employs nanotubes as nanoscale containers and reaction vessels.<sup>2</sup> The nano test tube’s yoctolitre volume allows researchers to sample molecules in very small quantities and study reactions at the

single molecule level using transmission electron microscopy (TEM). TEM is an indispensable tool for imaging molecules in direct space and real time, providing snapshots of reactions<sup>3–8</sup> or spatiotemporally continuous movies of molecular reactions.<sup>9–11</sup> However, TEM is an invasive technique with the electron beam transferring significant energy to the sample during imaging. When carefully controlled the electron beam can be harnessed to drive chemical reactions, an approach termed chemical TEM (ChemTEM), to provide a wealth of information on intermolecular reactions.<sup>12</sup> In general, electron beam activated processes are superimposed on any thermally activated processes, as demonstrated for the cases of fullerene dimerisation and polymerisation in nanotubes using the SMART-TEM approach.<sup>6,13</sup> The electron dose rate can be varied in a controlled fashion in order to quantitatively decouple thermal processes from those activated by the electron beam.<sup>14–16</sup> Here, we demonstrate a methodology that removes the impact of the electron beam on the reaction by using controlled variation of the sample temperature to thermally activate reactions. Chemical activation parameters are determined by directly counting individual reactant molecules in TEM images.

Perchlorocoronene (PCC) C<sub>24</sub>Cl<sub>12</sub> molecules are known to pack densely within carbon nanotubes, forming stacks with neighbouring molecules separated by van der Waals gaps (Fig. 1a). Such a regular, predictable arrangement of reactant molecules presents excellent imaging conditions in which each molecule can be accounted for as a 1.41 nm sharp, high-contrast line (Fig. 1b). The molecules can be accurately counted directly from TEM images without requiring atomic resolution. Our previous investigation of electron beam activated reactions of PCC showed that chemical transformations resulted in the molecules being removed from the ordered stack and forming new structures (e.g. dimers, oligomers, nanoribbons) that do not stack inside the nanotube.<sup>10</sup> Nanotube itself however is not involved in reactions with these guest-molecules, due to a low reactivity of the concave side of SWNT<sup>17</sup> which typically does not engage in reactions with polyaromatic molecules,<sup>18,19</sup> and there is no indication of the reactive species formed from PCC bonding the SWNT in this or the previous studies.<sup>10</sup>

<sup>a</sup> School of Chemistry, University of Nottingham, University Park, Nottingham NG7 2RD, UK.

<sup>b</sup> Electron Physical Sciences Imaging Centre, Diamond Light Source Ltd., Oxfordshire OX11 0DE, UK.

<sup>c</sup> Department of Materials, University of Oxford, Parks Road, Oxford OX1 3PH, UK.

\*A.N.K. email: andrei.khlobystov@nottingham.ac.uk

Electronic Supplementary Information (ESI) available. See DOI: 10.1039/x0xx00000x

Thermally activated reactions of PCC have been shown to occur in the bulk crystal at temperatures above 600 °C, and polymerisation of PCC stacks inside the nanotube can take place rapidly at 700 °C.<sup>10</sup> In order to derive information about thermally activated reactions, it is important to minimise the effect of the electron beam. PCC is known to be highly stable under electron irradiation, with no measurable changes observed up to doses of  $10^6 \text{ e}^- \text{ nm}^{-2}$  in the crystal and as high as *c.a.*  $2 \times 10^8 \text{ e}^- \text{ nm}^{-2}$  when encapsulated in carbon nanotubes.<sup>10,20</sup> The lowest electron dose we observed to trigger a reaction between PCC molecules was  $5.43 \times 10^6 \text{ e}^- \text{ nm}^{-2}$  (SI Fig. 1). In our experiments the cumulative electron dose was carefully controlled so that molecules experienced an average dose of  $1.92 \times 10^5 \text{ e}^- \text{ nm}^{-2}$  of 80 keV electrons, ensuring that reactions were driven entirely by thermal activation. The molecules experienced no irradiation prior to heating. Following heating, the products experienced a maximum dose of  $2.74 \times 10^5 \text{ e}^- \text{ nm}^{-2}$ , an order of magnitude lower than the minimum dose required to trigger a reaction at room temperature (SI Fig. 1).

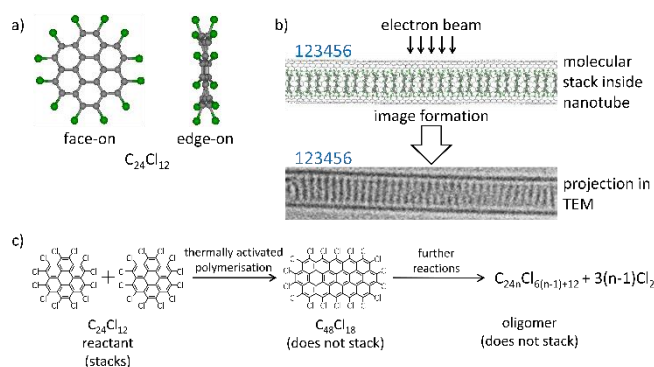


**Figure 1.** a) Face-on and edge-on structural diagrams of perchlorocoronene (PCC). b) A phase contrast HRTEM image of PCC@SWNT where individual molecules can be counted. c) Thermally activated reactions of PCC produce oligomers and polymers that do not stack within SWNTs and thus can be easily distinguished from PCC reactant molecules.

PCC@SWNT was deposited onto three separate TEM heating chips (DENS Solutions Wildfire) for each temperature (500, 550, and 600 °C). The local temperature of the sample is controlled by heating coils embedded in the TEM chip with 99.5% temperature homogeneity across the sample area. In each heating cycle, the temperature of the sample was ramped up to the desired temperature within a minute (either 500, 550, or 600 °C) and held at that temperature for 5 min, followed by cooling to ambient temperature (23 °C). The sample was allowed to equilibrate for another 5 min before un-blanking the electron beam to acquire images of fresh, non-irradiated areas. The heating-imaging cycle was repeated three times for each sample at the three temperatures (hence requiring three different heating chips), resulting in total heating times of 5, 10, and 15 min (Fig. 2). Under these experimental conditions, all observable changes in PCC are driven by the thermally induced reactions, described by a reaction rate constant of  $k_T$  (Scheme 1).

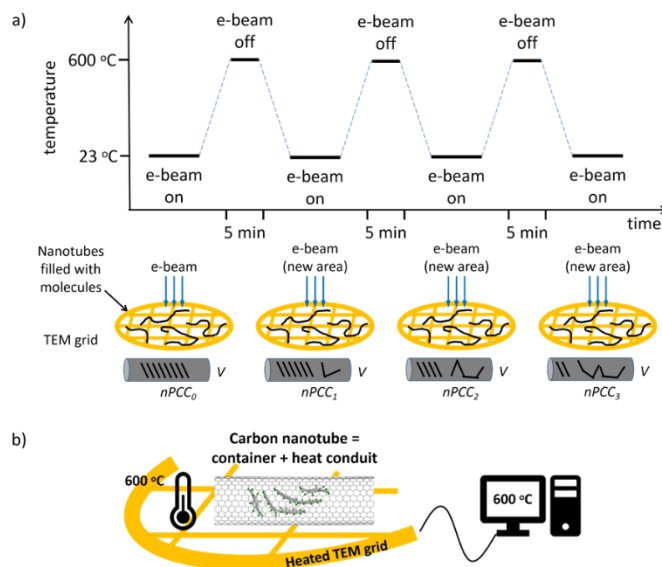
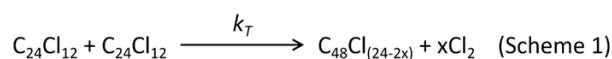


**Figure 2.** a) Each heating cycle consists of a quick ramp (tens of seconds) up to the desired temperature (either 500, 550, or 600 °C) and a dwell at that temperature for 5 min, followed by cooling to ambient temperature (23 °C) and equilibration for another 5 min. The electron beam is then un-blanked to acquire images of fresh, non-irradiated areas. The number of reactant molecules  $n\text{PCC}$  in a volume  $V$  of nanotube can be counted directly from the images. b) Separate heating chips were used for each experiment with a given elevated temperature. For each of the three temperatures, three heating cycles were carried out, giving three data points at each temperature corresponding to 5, 10, and 15 min of heating in total.

High magnification TEM imaging demonstrates that reactions of PCC take place at all three temperatures to different extents. The resulting polymeric products are quite disordered and not well-defined structurally (Fig. 3a), reminiscent of Diels-Alder cycloadducts of PCC that precede the formation of nanoribbons during prolonged heating to 700–900 °C or extensive electron beam irradiation.<sup>10</sup> Importantly, at all three temperatures, 500, 550, and 600 °C, intact reactant molecules of PCC can still be found (Fig. 3a). These observations are consistent with the previous report that the full thermal conversion of all PCC molecules and structural annealing to a zigzag nanoribbon can only be achieved by heating to 700 °C or higher for 24 hours.<sup>10</sup>

Images were first taken at 23 °C to determine the number of PCC molecules ( $n\text{PCC}_0$ ) per volume of nanotube ( $V$ ),  $n\text{PCC}_0/V$ , prior to reaction (SI sections 1 and 2). PCC was observed to stack densely within SWNT cavities with no extended gaps between the molecules (Fig. 1b) suggesting the same initial concentration of the reactant molecules in all nanotubes before heating. The number of molecules per nanotube volume,  $n\text{PCC}/V$ , was then determined after each stage of the heating cycle. These values were used to determine the thermally driven reaction rate constant  $k_T$ , taking into account the length of time of the heating (SI section 3). Each value of  $k_T$  was directly determined from an average number of molecules per volume

$nPCC/V$  taken from 3-13 individual nanotubes at each temperature (500, 550, and 600 °C) and the length of time taken for heating (5, 10, and 15 min).

The second order rate equation for the reaction shown in Scheme 1 can be written as:

$$-\frac{d(nPCC/V)}{dt} = \left(\frac{2}{x+1}\right) k_T (nPCC_0/V)^2 \quad (\text{Equation 1})$$

where  $nPCC_0/V$  is the initial number of PCC molecules per volume of nanotube and  $x$  is the number of moles of  $Cl_2$ .

Loss of  $Cl_2$  during heating produces reactive species such as radicals and arynes of PCC. Reactions between such reactive species are highly likely to occur at elevated temperatures, even after loss of only one mole of  $Cl_2$ . Therefore, the second order rate equation can be simplified to the integrated rate equation:

$$\frac{1}{(nPCC/V)} = k_T t + \frac{1}{(nPCC_0/V)} \quad (\text{Equation 2})$$

The Eyring equation can be used to interpret the temperature dependence of second-order rate constants:

$$k_T = \frac{k_B T}{h} \exp\left(-\frac{\Delta G^\ddagger}{k_B T}\right) = \frac{k_B T}{h} \exp\left(-\frac{\Delta H^\ddagger}{k_B T} + \frac{\Delta S^\ddagger}{k_B}\right) \quad (\text{Equation 3})$$

where  $k_T$  is the second-order rate constant,  $k_B$  is Boltzmann's constant ( $1.381 \times 10^{-23} \text{ J K}^{-1}$ ),  $h$  is Planck's constant ( $6.626 \times 10^{-34} \text{ J s}$ ),  $T$  is the temperature in K,  $\Delta G^\ddagger$  is the Gibbs free energy of activation,  $\Delta H^\ddagger$  is the enthalpy of activation, and  $\Delta S^\ddagger$  is the entropy of activation.

By plotting the experimental data as  $\ln(k_T/T)$  against  $1/T$  (using Fig. 3b), a clear thermal dependence of  $k_T$  is revealed, giving  $\Delta H^\ddagger$  as  $104.3 \pm 10.2 \text{ kJ mol}^{-1}$  ( $1.08 \pm 0.11 \text{ eV}$  per molecule) and  $\Delta S^\ddagger$  as  $-0.163 \pm 0.185 \text{ kJ mol}^{-1} \text{ K}^{-1}$  ( $-39.08 \pm 44.25 \text{ cal mol}^{-1} \text{ K}^{-1}$ ).  $\Delta G^\ddagger$  can therefore be calculated for each temperature used, resulting in the range 231-247  $\text{kJ mol}^{-1}$  across 500-600 °C (Fig. 3b; standard deviations for each parameter in SI section 3, Table 5).<sup>21</sup> The activation energies of irreversible solid-state polymerisations are typically in the range of 33-330  $\text{kJ mol}^{-1}$ .<sup>22</sup> The barrier we have determined for PCC polymerisation in nanotubes falls at the upper end of this range, which is expected considering the high thermal stability of the PCC molecule in bulk.<sup>20</sup>

$$\ln\left(\frac{k_T}{T}\right) = -\frac{\Delta H^\ddagger}{k_B} \cdot \frac{1}{T} + \ln\left(\frac{k_B}{h}\right) + \frac{\Delta S^\ddagger}{k_B} \quad (\text{Equation 4})$$

It is worth commenting on our use of the Eyring equation rather than the Arrhenius equation to calculate activation parameters. In addition to being more suitable for solid-state reactions, the Eyring approach has the advantage of explicitly giving separate enthalpic and entropic contributions to the reaction barrier,

rather than a single empirical activation energy. While this is generally useful, for the type of nanoconfined reaction studied here it is crucial, as entropic effects play an important role due to the reduction in translational and rotational degrees of freedom of reactant molecules upon encapsulation into the nanotube.<sup>23,24</sup> Across our reaction temperature range, we estimate that this effect would make the free energy of a reactant PCC molecule more positive by approximately 105-127  $\text{kJ mol}^{-1}$ . From our experimentally measured values, the entropic term is responsible for 126-143  $\text{kJ mol}^{-1}$  of the Gibbs free energy of activation, corresponding to 55-58% of the barrier. An Arrhenius approach in this case would result in activation energies that are misleadingly low (only 63.5  $\text{kJ mol}^{-1}$ ) when conceptually taken as the reaction 'barrier'; this approach and further discussion of the entropic contribution is included in SI section 4.

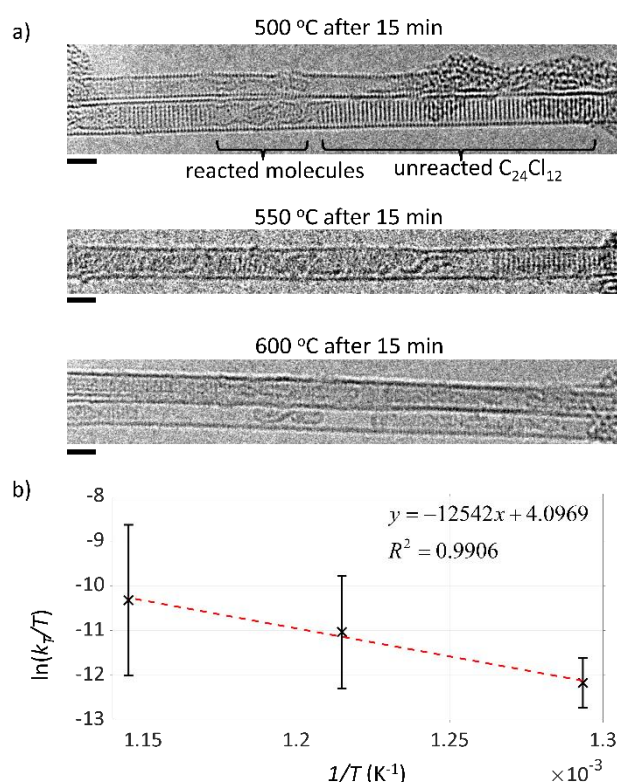


**Figure 3.** a) The polymerisation products after heating for 15 min at 500, 550, and 600 °C. Polymerisations occurred at several points along the SWNTs, as can be seen from products that are distinct from the reactant PCC molecules. The scale bars are 1 nm. b) The enthalpy of activation  $\Delta H^\ddagger$  and entropy of activation  $\Delta S^\ddagger$  can be calculated for the thermally induced polymerisation of PCC using a linear plot of  $\ln(k_T/T)$  against  $1/T$  (Eq. 4). Error bars show the standard deviation of the average  $\ln(k_T/T)$  (details are in SI section 3 Table 4).

We have measured the activation parameters of a thermally driven reaction by counting individual molecules in nano test tubes directly from TEM images. The effects of the electron beam – a substantial confounding factor in TEM studies of molecules – were minimised by designing a careful heating and imaging protocol in which the electron dose per molecule was

kept an order of magnitude lower than the minimum dose required for the onset of electron beam induced reactions at room temperature. In contrast to molecular or atomic kinetics studies in the TEM in which the electron beam is the driving force of the reaction,<sup>13,25-27</sup> here the reaction was driven by heat. This allowed us to obtain  $\Delta H^\ddagger$ ,  $\Delta S^\ddagger$ , and  $\Delta G^\ddagger$ , parameters that are relevant to traditional chemical kinetics on the macroscale, through direct imaging of the chemical reaction. A key advantage of this methodology over previous approaches<sup>14-16</sup> of decoupling electron beam and thermal processes is that by only allowing the thermal reaction to take place and varying the temperature, we can directly measure the activation parameters rather than only the rate constant  $k_T$ . There is no need for prior knowledge of the value of the Arrhenius prefactor, and consideration of the enthalpic and entropic contributions to the barrier provides additional insight into the chemical reaction.

This method of directly counting reactant molecules is applicable to reactions where individual molecules can be clearly imaged by TEM, remain stable under the electron beam during image capture, and are sufficiently distinct from products of the reaction. As the key measurable quantity from the TEM images is the number of molecules per volume, the presence of a fixed volume imposed by a well-defined host (e.g. a nano test tube) is also of practical importance. Further developments in TEM camera technologies, such as direct electron detectors, have the potential to substantially extend the range of molecules and reactions to which this approach can be applied. The proliferation of accurate heating holders and chips is vital to enable the study of reaction kinetics in the TEM, while improvements in the accuracy, precision, and speed of temperature control will reduce the uncertainties in the measured activation parameters. Future development of low-dose TEM imaging methods, combined with heated sample supports, will allow for spatiotemporally continuous observation of thermally driven reactions at the single-molecule level, thus enabling the elucidation of atomistic mechanisms and discovery of new types of reactions.

We thank Diamond Light Source for access and support in use of the electron Physical Science Imaging Centre (Instrument E02 and proposal numbers MG22887, MG23260, and MG25251), S. Aslam for assistance with <sup>13</sup>C NMR spectroscopy, and the Nanoscale & Microscale Research Centre (nmRC) for access to materials characterisation instrumentation. A.N.K. acknowledges support from the Engineering and Physical Sciences Research Council (EPSRC).

There are no conflicts to declare.

## Notes and references

1. P. Hinterdorfer and A. van Oijen, Eds., *Handbook of Single-Molecule Biophysics*, Springer US, New York, 2009.
2. D. A. Britz, A. N. Khlobystov, K. Porfyrakis, A. Ardavan and G. A. D. Briggs, *Chem. Commun.*, 2005, 37-39.
3. D. E. Luzzi and B. W. Smith, *Carbon*, 2000, **38**, 1751-1756.
4. A. Chuvilin, A. N. Khlobystov, D. Obergfell, M. Haluska, S. Yang, S. Roth and U. Kaiser, *Angew. Chem. Int. Ed.*, 2010, **49**, 193-196.
5. G. Brown, S. R. Bailey, J. Sloan, C. Xu, S. Friedrichs, E. Flahaut, K. S. Coleman, J. L. Hutchison, R. E. Dunin-Borkowski and M. L. H. Green, *Chem. Commun.*, 2001, 845-846.
6. M. Koshino, Y. Niimi, E. Nakamura, H. Kataura, T. Okazaki, K. Suenaga and S. Iijima, *Nat. Chem.*, 2010, **2**, 117-124.
7. S. Gorantla, F. Börrnert, A. Bachmatiuk, M. Dimitrakopoulou, R. Schönfelder, F. Schäffel, J. Thomas, T. Gemming, E. Borowiak-Palen, J. H. Warner, B. I. Yakobson, J. Eckert, B. Büchner and M. H. Rümmeli, *Nanoscale*, 2010, **2**, 2077-2079.
8. C. Jin, H. Lan, K. Suenaga, L. Peng and S. Iijima, *Phys. Rev. Lett.*, 2008, **101**, 176102.
9. J. Biskupek, S. T. Skowron, C. T. Stoppiello, G. A. Rance, S. Alom, K. L. Y. Fung, R. J. Whitby, M. H. Levitt, Q. M. Ramasse, U. Kaiser, E. Besley and A. N. Khlobystov, *ACS Nano*, 2020, **14**, 11178-11189.
10. T. W. Chamberlain, J. Biskupek, S. T. Skowron, A. V. Markevich, 11. S. Kurasch, O. Reimer, K. E. Walker, G. A. Rance, X. Feng, K. Mullen, A. Turchanin, M. A. Lebedeva, A. G. Majouga, V. G. Nenajdenko, U. Kaiser, E. Besley and A. N. Khlobystov, *ACS Nano*, 2017, **11**, 2509-2520.
12. K. Cao, S. T. Skowron, J. Biskupek, C. T. Stoppiello, C. Leist, E. Besley, A. N. Khlobystov and U. Kaiser, *Sci. Adv.*, 2020, **6**, eaay5849.
13. S. T. Skowron, T. W. Chamberlain, J. Biskupek, U. Kaiser, E. Besley and A. N. Khlobystov, *Acc. Chem. Res.*, 2017, **50**, 1797-1807.
14. S. Okada, S. Kowashi, L. Schweighauser, K. Yamanouchi, K. Harano and E. Nakamura, *J. Am. Chem. Soc.*, 2017, **139**, 18281-18287.
15. S. T. Skowron, V. O. Koroteev, M. Baldoni, S. Lopatin, A. Zurutuza, A. Chuvilin and E. Besley, *Carbon*, 2016, **105**, 176-182.
16. M. S. Isaacson, J. Langmore, N. W. Parker, D. Kopf and M. Utlaut, *Ultramicroscopy*, 1976, **1**, 359-376.
17. M. S. Isaacson, D. Kopf, M. Utlaut, N. W. Parker and A. V. Crewe, *Proc. Natl. Acad. Sci.*, 1977, **74**, 1802-1806.
18. Z. Chen, W. Thiel and A. Hirsch, *ChemPhysChem*, 2003, **1**, 93-97.
19. T. W. Chamberlain, J. Biskupek, S. T. Skowron, P. A. Baylis, E. Bichoutskaia, U. Kaiser and A. N. Khlobystov, *Small*, 2015, **11**, 622-629.
20. B. Botka, M. E. Füstös, H. M. Tóháti, K. Németh, G. Klupp, Z. Szekrényes, D. Kocsis, M. Utzcs, E. Székely, T. Váczi, G. Tarczay, R. Hackl, T. W. Chamberlain, A. N. Khlobystov, K. Kamarás, *Small*, 2014, **10**, 1369-1378.
21. M. Koshino, H. Kurata and S. Isoda, *Ultramicroscopy*, 2010, **110**, 1465-1474.
22. G. Lente, I. Fábián and A. J. Poë, *New J. Chem.*, 2005, **29**, 759-760.
23. S.N. Vouyiouka, E.K. Karakatsani and C.D. Papaspyrides, *Prog. Polym. Sci.*, 2005, **30**, 10-37.
24. S. A. Miners, G. A. Rance and A. N. Khlobystov, *Chem. Soc. Rev.*, 2016, **45**, 4727-4746.
25. T. S. Koblenz, J. Wassenaar and J. N. H. Reek, *Chem. Soc. Rev.*, 2008, **37**, 247-262.
26. J. C. Meyer, F. Eder, S. Kurasch, V. Skakalova, J. Kotakoski, H. J. Park, S. Roth, A. Chuvilin, S. Eyhusen, G. Benner, A. V. Krashenninnikov and U. Kaiser, *Phys. Rev. Lett.*, 2012, **108**, 196102.
27. J. Kotakoski, C. Mangler and J. C. Meyer, *Nat. Commun.*, 2014, **5**, 3991.
28. S. Kretschmer, T. Lehnert, U. Kaiser and A. V. Krashenninnikov, *Nano Lett.*, 2020, **20**, 2865-2870.